Electrochimica Acta 107 (2013) 9–15

Contents lists available at ScienceDirect

Electrochimica Acta

journal homepage: www.elsevier.com/locate/electacta

Synthesis of porous NiO using $NaBH_4$ dissolved in ethylene glycol as precipitant for high-performance supercapacitor☆

Miaomiao Liu, Jie Chang, Jing Sun*, Lian Gao

The State Key Lab of High Performance Ceramics and Superfine Microstructure, Shanghai Institute of Ceramics, Chinese Academy of Sciences, 1295 Ding Xi Road, Shanghai 200050, China

ARTICLE INFO

Article history:
Received 18 March 2013
Received in revised form 15 May 2013
Accepted 31 May 2013
Available online 14 June 2013

Keywords:
NiO
$NaBH_4$
Ethylene glycol
Electrode material
Supercapacitor

ABSTRACT

A facile reflux method has been developed to prepare porous NiO samples using $NaBH_4$-EG and NaOH-EG as alkaline precipitants, respectively. $NaBH_4$-EG is used as alkaline precipitant for the first time. Precipitants influence the morphology and structure of NiO significantly, further affect their specific capacitances as supercapacitor electrodes. Compared with NaOH, $NaBH_4$-EG as alkaline precipitant shows great superiority on morphology control. NiO synthesized by $NaBH_4$-EG presents spherical spongy shape with high specific surface areas, whereas the sample synthesized by NaOH-EG exhibits agglomerated irregular structure. When being applied as supercapacitor electrodes, the former NiO could achieve an extremely high specific capacitance of 930 $F g^{-1}$ at a current density of 15 $A g^{-1}$, significantly higher than that of the latter one (510 $F g^{-1}$). Moreover, the specific capacitance of the former is as high as 1396 $F g^{-1}$ after 1000-cycle at 4 $A g^{-1}$, revealing superb electrochemical characteristics. The impedance measurement discloses that the electrode prepared by the former NiO possesses lower charge-transfer resistance and ion-diffusion resistance, demonstrating the superiority of $NaBH_4$-EG as alkaline precipitant. $NaBH_4$-EG is an excellent precipitant for the synthesis of porous NiO as supercapacitor electrodes.

1. Introduction

It is urgent to develop new and efficient energy-storage devices to resolve the present energy and environmental problems caused by the depleting of fossil fuels [1–6]. As one of the highly promising candidates, electrochemical supercapacitors have attracted much attention due to high power density, low maintenance cost, and long cycling lifetime [6–9]. However, they usually suffer from a lower energy density than rechargeable batteries [10]. It is a major topic of interest to prepare new materials which deliver high power and energy density simultaneously. Based on the charge storage mechanisms, supercapacitors broadly include electrical double layer capacitors (EDLCs) and pseudocapacitors [11]. The poor energy density of EDLCs limits their practical applications. Transition metal oxides and conductive polymers used as pseudocapacitors show high specific capacitance and energy density owing to Faradic redox reactions, therefore they have been investigated widely [12,9]. Among them, RuO_2, with a specific capacitance of 1580 $F g^{-1}$, has been considered as the most promising material for the next generation supercapacitors [13]. However, the high cost of RuO_2 hampers their commercial application. In this respect, a broad range of low cost alternative materials with excellent performance, such as NiO [14–19], $Ni(OH)_2$ [20–23], Co_3O_4 [24,25], MnO_2 [26,27] and $NiCo_2O_4$ [28], have been actively pursued. Of all these, NiO is a potential electrode material by virtue of its low cost, environmentally benign nature and high theoretical specific capacitance.

Since the Faradaic electrochemical processes occur only on the surface and near surface of pesudocapacitance materials, surface properties including morphology, specific surface area, and pore size distribution play a key role in the charge storage processes [14]. Thus, lately a number of efforts have been paid to optimize the morphology of NiO to enhance their specific capacitance [29]. Of all the efforts, hierarchical porous NiO has been prepared by various methods as research hotspot [6,29–34]. For example, Cao et al. [16] developed microwave-assisted methods for making flower-like NiO with the specific capacitance of 585 $F g^{-1}$ at 5 $A g^{-1}$. Zhang et al. [29] prepared various porous NiO with adjustable surface area, and a specific capacitance of 390 $F g^{-1}$ was attained at 5 $A g^{-1}$. Li et al. [31] synthesized mesoporous NiO by hydrothermal method, achieving the specific capacitance of 555 $F g^{-1}$ at 2 $A g^{-1}$. However, complicated equipments were needed in the above processes and the specific capacitance of NiO was not as high as expected.

In this work, NiO has been prepared by a reflux method using $NaBH_4$-EG as alkaline precipitant. $NaBH_4$, well-known as a reductant is rarely used as alkaline precipitant [35]. $NaBH_4$ dissolved in ethylene glycol is used as alkaline precipitant for the first time

* Corresponding author. Tel.: +86 12 52414301; fax: +86 21 52413122.
E-mail address: jingsun@mail.sic.ac.cn (J. Sun).

0013-4686/$ – see front matter © 2013 The Authors. Published by Elsevier Ltd. All rights reserved.
http://dx.doi.org/10.1016/j.electacta.2013.05.122

in this study. By dissolving $NaBH_4$ in ethylene glycol, it worked as a good precipitant to prepare homogeneous porous NiO. The resulting sample shows nanoflakelets constituted spherical spongy structure with large specific surface areas. An extremely high capacitance of 1030 F g^{-1} is achieved at 0.5 A g^{-1}, and it can be maintained 930 F g^{-1} at 15 A g^{-1}.

2. Experimental

2.1. Materials preparation

Typically, 1.2 g $NaBH_4$ was dissolved in 25 mL ethylene glycol (EG) until the bubbling ended, forming $NaBH_4$-EG solution. 600 mg $Ni(NO_3)_2{\cdot}6H_2O$ dissolved in 100 mL EG was heated to 190 °C, to which $NaBH_4$-EG solution was added (Fig. S1). The mixture was kept stirring at 190 °C for 1 h. After reaction, the sample was washed with distilled water and ethanol for several times and then dried at 100 °C overnight. The as-prepared sample was further calcined at 250 °C for 2 h in air to obtain NiO. As comparison, NiO was synthesized by the same procedure except substituting $NaBH_4$ with NaOH. The two kinds of NiO were denoted as NiO–$NaBH_4$ and NiO–NaOH, respectively. For the FTIR characterization, the above $NaBH_4$-EG solution was dried in vacuum at 170 °C to form dry powder, named dry $NaBH_4$-EG.

2.2. Materials characterization

The phase of the products was examined by X-ray powder diffraction (XRD) on Rigaku D/Max-2550V diffractometer using Cu Kα radiation. The morphology of the products was observed on a transmission electron microscope (TEM 30 JEOL JEM-2100F) and a scanning electron microscope (SEM JEOL S-4800). The specific surface area was investigated by Brunauer–Emmett–Teller (BET) method at 77 K in N_2 (V-Sorb 2800P, Gold APP, China). The pore size distributions were calculated from desorption branches of the isotherms by Barrett–Joyner–Halenda (BJH) method. FTIR was recorded on a Nicolet 7000-C, Thermal Scientific Co., USA.

2.3. Electrochemical measurements

The working electrodes were prepared by mixing the as-prepared NiO, acetylene black and polytetrafluoroethylene (PTFE) binder (weight ratio of 70:20:10), and pressing onto a nickel foam (1 cm × 1 cm) current collector. Each working electrode contained about 3 mg of electrode material. All the electrochemical measurements were performed in a three-electrode system. The working electrode was dipped into 2 M KOH aqueous solution. A platinum wire and a saturated calomel electrode (SCE) were used as the counter electrode and the reference electrode, respectively. Cyclic voltammetry (CV) and electrochemical impedance spectroscopy (EIS) were carried out on a Parstat 2273 electrochemical station (Princeton applied research CO. Ltd., USA). EIS measurements were conducted in the frequency range from 0.01 to 100 kHz at a constant dc bias potential of 0.2 V with an ac perturbation of 5.0 mV. Galvanostatic charge/discharge tests were performed on a LAND CT2001A cell 50 measurement system.

3. Results and discussion

3.1. $NaBH_4$ dissolved in EG as alkaline precipitant

The hydrogen proton of EG is active, which reacts with $NaBH_4$ easily. When $NaBH_4$ was added in EG, the solution bubbled violently, along with strong heat released, and verifying the reaction occurred between them. In order to disclose the reaction mechanism, the FTIR of $NaBH_4$ and $NaBH_4$-EG were collected. As seen from Fig. S2, the peaks around 2387, 2229, and 2224 cm^{-1} are strong for pure $NaBH_4$, attributed to the vibrational bands of B—H. For comparison, these peaks of dry $NaBH_4$-EG are weaker, indicating the weakened reducibility of $NaBH_4$. At the same time, some new vibrational peaks of C—H, C—O and B—O appear, demonstrating the generation of a new substance. The possible reaction is as follows.

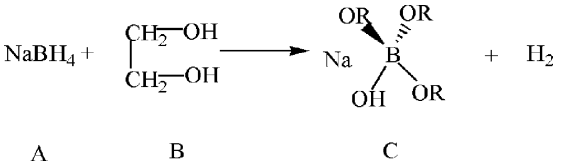

A B C

$NaBH_4$ reacts with EG, generating H_2 and a kind of Lewis base (C) (pH ≈ 9.6). From the FTIR spectra, we can figure out that the weak base is a complex macromolecule. However, the exact reaction mechanism would be determined after further investigation.

3.2. Nickel alkoxide precursor characterization

In order to analyze the as-prepared precursors, a series of characterization were carried out. The powder XRD patterns of the precursors, shown in Fig. S3, disclosed the characteristic peaks at around 10°, which is a standard pattern for metal alkoxide [36]. In the Fourier transform IR (FTIR) spectra (Fig. S4), the peaks around 2858, and 1084 cm^{-1} are ascribed to the vibrational bands of CH_2—, and C—OH, respectively, which further confirm that the as-prepared precursors are nickel alkoxide [37].

Thermogravimetric analysis was performed (Fig. S5) to determine the calcining temperature of nickel alkoxide precursors. The weight loss occurs in two temperature ranges: (i) 50–200 °C and (ii) 200–300 °C. The first weight loss occurred before 200 °C is attributed to the removal of adsorbed and intercalated solvent. For the two kinds of precursors, the mass losses are significantly distinct, demonstrating the different amount of adsorbed and intercalated solvent. The morphology influences the specific surface areas, further controls the amount of adsorbed and intercalated solvent. Nickel alkoxide precursor prepared by $NaBH_4$-EG presents more weight loss, indicating its larger specific surface areas and porous structure. The second mass loss corresponds to the decomposition of precursors. There is no obvious difference between the two mass losses, confirming the identical chemical compositions of precursors.

3.3. Nickel oxide characterization

After being calcined at 250 °C, both samples present five peaks in the XRD pattern, indexed to (1 1 1), (2 0 0), (2 2 0), (3 1 1), and (2 2 2) planes in the standard NiO spectrum (PDF#47-1049) (Fig. 1). No other peaks are observed, proving the pure phase of the samples. It is worth to note that the relative intensity and broadness of the diffraction patterns are distinct, indicating the different crystallite size and crystallinity of the two kinds of NiO. The XRD peaks of NiO–$NaBH_4$ are broader, testifying its smaller crystallite size. NiO–NaOH shows more intense peak, disclosing its better crystallinity.

The morphology and microstructure of NiO samples were characterized by SEM and TEM. As illustrated in Fig. 2a and b, NiO–$NaBH_4$ is composed of highly homogenous spherical spongy shape with the size of 200–300 nm. Each ball is bestrewed with many rippled-shaped interconnected thin nanoflakelets. NiO–NaOH (Fig. 2c and d) shows agglomerated irregular blocks, the size of which is larger than that of NiO–$NaBH_4$. Besides, the structure of NiO–NaOH is denser compared with NiO–$NaBH_4$. To observe inner structures of NiO samples, TEM image is given in Fig. 3. NiO–$NaBH_4$ has the nanoflake unites, forming porous structure (Fig. 3a). The irregular structure of NiO–NaOH consists of randomly

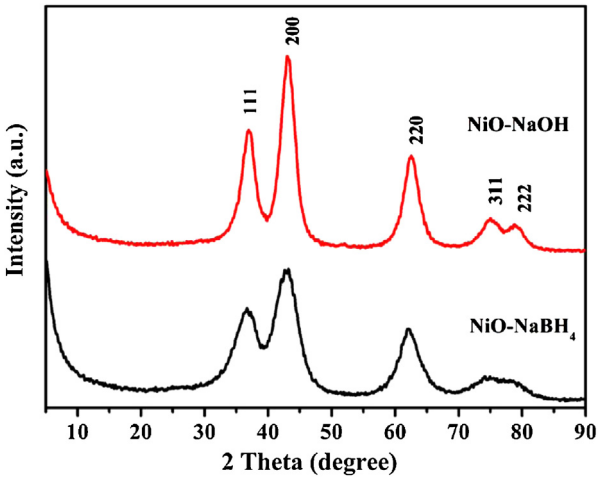

Fig. 1. XRD patterns of NiO samples.

aggregated particles of ~5 nm (Figs. 3c and S6). The selected-area electron diffraction (SAED) patterns of NiO samples are inseted in Fig. 3a and c. The rings indexed to the (1 1 1), (2 0 0), (2 2 0), and (3 1 1) planes of NiO, in consistent with the XRD data. The two HRTEM images (Fig. 3b and d) show the lattice distance of 0.21 nm, corresponding to the (2 0 0) plane of NiO.

Alkaline precipitants play key roles in the reaction process. No apparent precipitates formed without adding alkaline precipitants under the same procedure. Moreover, the different morphology of both NiO is attributed to the alkalinity of precipitants. As a strong alkaline, NaOH-EG provides high concentration of hydroxide ion which would form precursor particles of ~5 nm fast, and then formed irregular blocks through mass transport and directional fusion of particles (Fig. S7a). $NaBH_4$, a well-known reductant, is rarely used as alkaline precipitant. Lu et al. [35] prepared nickel nanoparticles successfully through reducing nickel chloride by solid $NaBH_4$. Interestingly, $NaBH_4$ dissolved in EG, generates a new Lewis base, namely C. This mild alkaline complex, with a macromolecular structure, is helpful to form precursor slowly and uniformly (Fig. S7b).

To better investigate the formation process of the porous structure, time-dependent experiments were carried out, during which the precursors were collected at different time intervals. Fig. 4 discloses the morphology evolution of the nickel alkoxide precursors prepared by $NaBH_4$-EG. The reaction of 4 min leads to the formation of nanoflakelets which are interconnected with each other randomly (Fig. 4a). This structure can be ascribed to the new macromolecular precipitant. On one hand, the new precipitant is a mild base (pH ≈ 9.6), which is helpful for the generation of nickel alkoxide. On the other hand, the macromolecule, as a kind of structure-directing agent results in the forming of flakelet structure. When the reaction time is 10 min, the shape of precursor does not change greatly while the nanoflakelets are more clearly (Fig. 4b). As seen from Fig. 4c, spherical spongy structure formed through the assembling of the nanoflakelets at the reaction time of 30 min. With the prolongation of reaction time, the regular spherical spongy structure becomes clearer. The nickel alkoxide precursor finally forms complete uniform spherical spongy structure at the reaction time of 1 h (Fig. 4d). Based on the above experiments, the following mechanism is proposed (Fig. 5). The whole reaction process can be divided into three steps: (i) formation and random agglomeration of nanoflakelets, (ii) self-assembly of nanoflakelets to incomplete ball-like structure and (iii) growth of complete uniform ball-like structure.

BET analysis was investigated to study the porous structure of NiO samples. Nitrogen adsorption/desorption isotherms and BJH pore size distribution plots of NiO samples are presented in Fig. 6. The specific surface areas are determined to be 414 $m^2 g^{-1}$ and 220 $m^2 g^{-1}$ for NiO–$NaBH_4$ and NiO–NaOH, respectively. The corresponding pore size distributions plots given in the insets state that the pore sizes are 3–4 and 4–7 nm calculated by the BJH method. The higher surface area of NiO–$NaBH_4$ can be ascribed to spongy structure and narrower pore size distribution. As well known, the large specific surface area and suitable pore size distribution in the range of 2–5 nm is favorable for electrochemical reaction [29,38]. Zhang et al. has prepared porous NiO nanoslice,

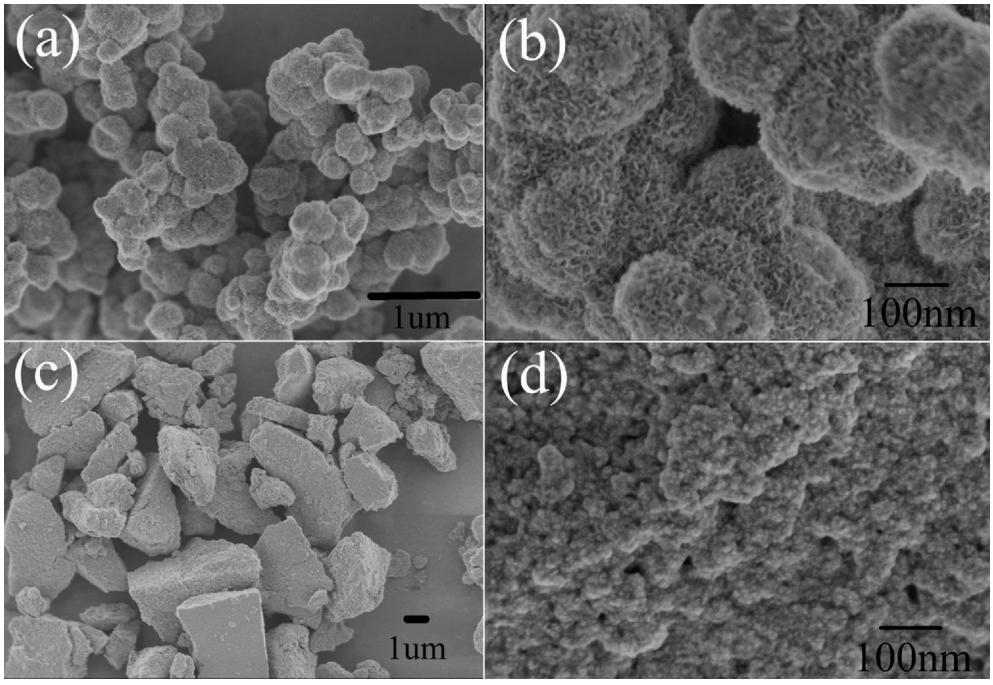

Fig. 2. (a) Low- and (b) high-resolution SEM images of NiO–$NaBH_4$. (c) Low- and (d) high-resolution SEM images of NiO–NaOH.

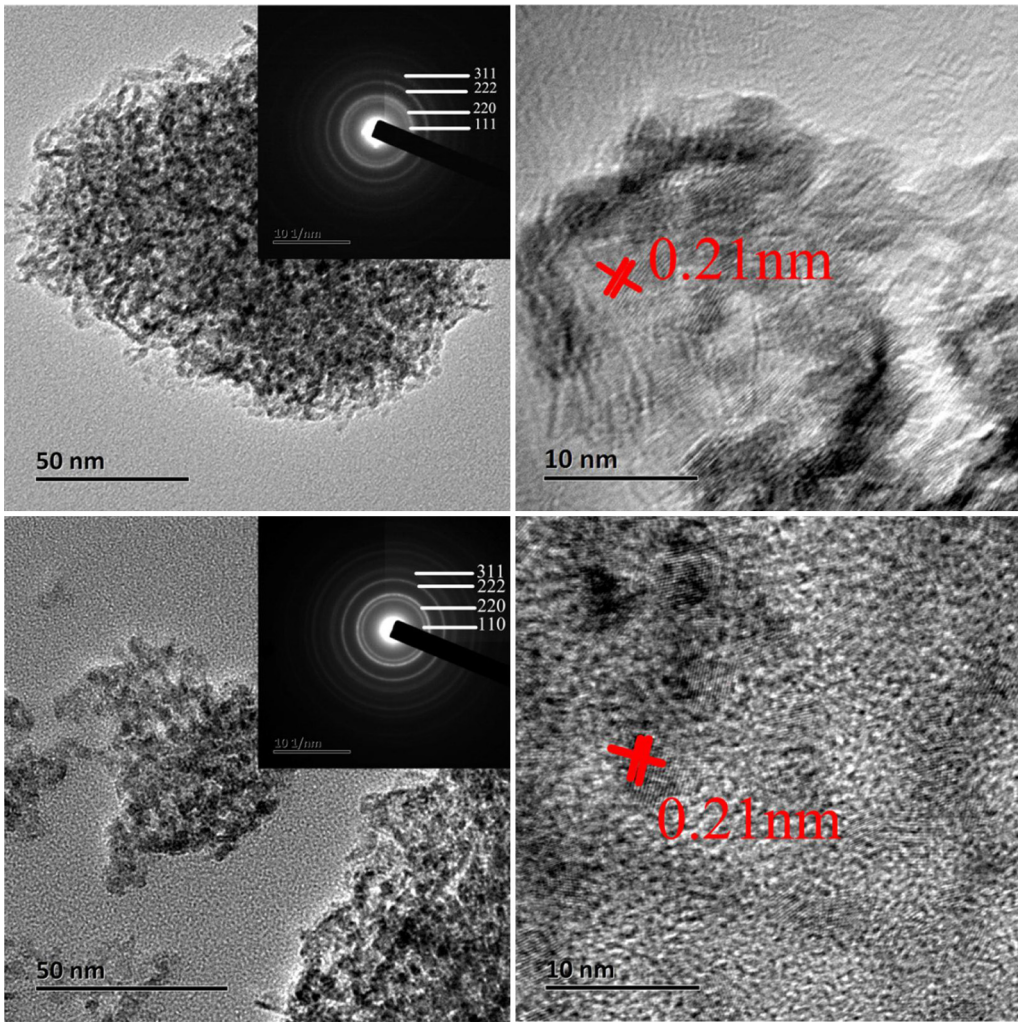

Fig. 3. (a) TEM and (b) HRTEM images of NiO–$NaBH_4$. (c) TEM and (d) HRTEM images of NiO–NaOH. The insets are the corresponding SAED patterns of NiO–$NaBH_4$ and NiO–NaOH.

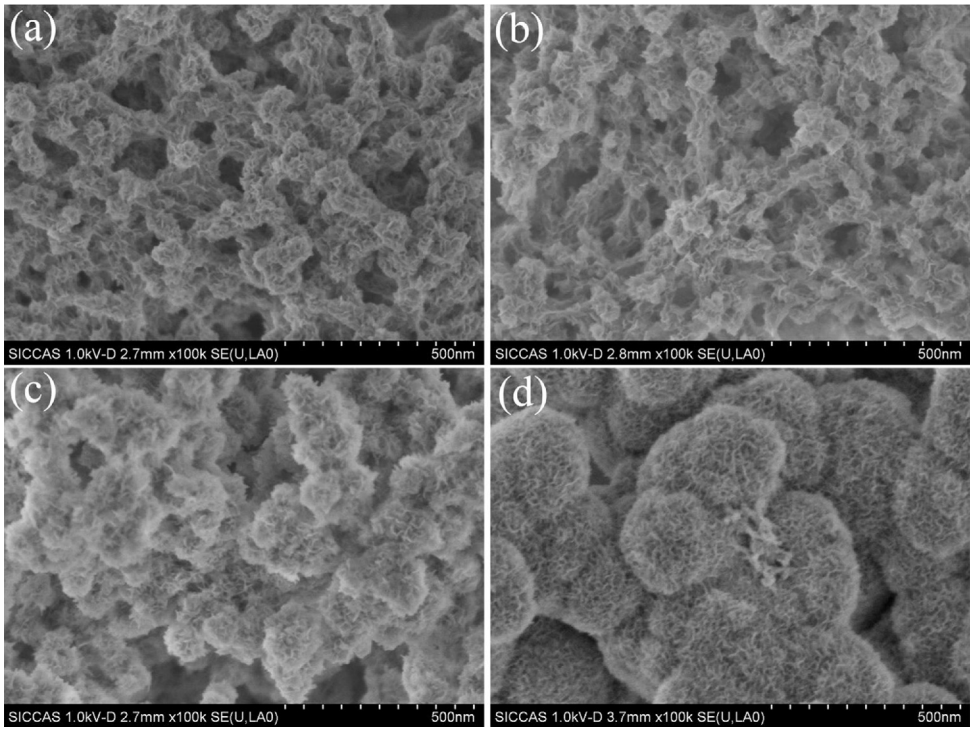

Fig. 4. SEM images of the nickel oxide precursors grown for (a) 4 min, (b) 10 min, (c) 30 min, and (d) 1 h.

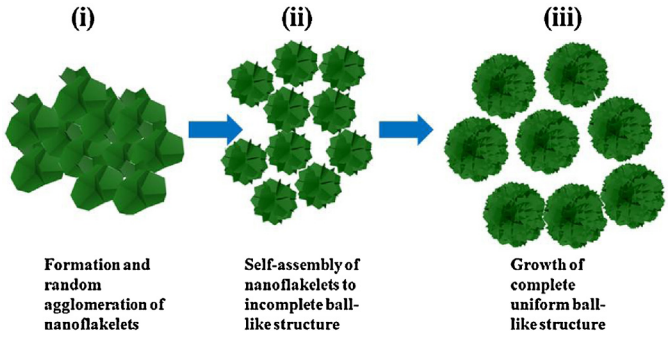

Fig. 5. Schematic procedure for the formation mechanism of ball-like spongy structure.

nanoplates and nanocolumns with different specific surface areas and pore size distribution. Their experiment has proved that NiO nanocolumns with larger specific surface areas and smaller pore size distribution possessed the best performance. The large specific surface areas can provide the high availability of electrode materials to electrolyte. Meanwhile, the appropriate pore size facilitates better diffusion and accession of electrolyte ions through pore channels for efficient redox reactions during the charge storage process. From this point, NiO–$NaBH_4$, with larger specific surface area and more appropriate pore size distribution, is a better electrode material than NiO–NaOH. To confirm this, the electrochemical performances of both kinds of NiO samples have been studied by cyclic voltammetry, galvanostatic charge/discharge, and electrochemical impedance spectroscopy.

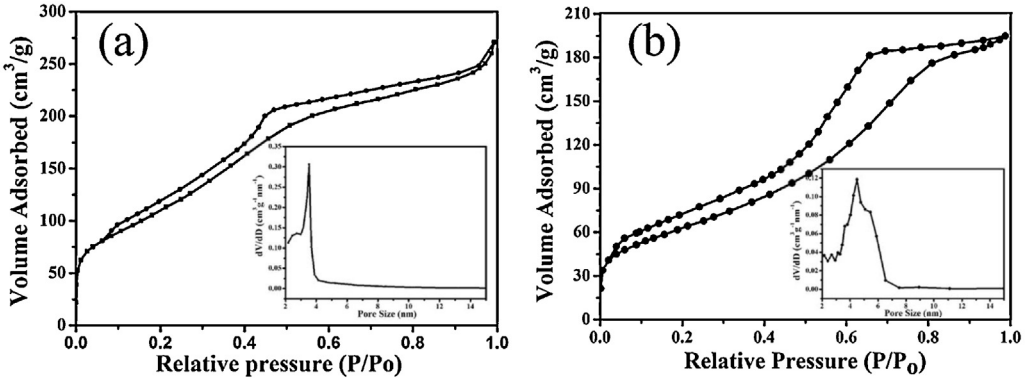

Fig. 6. Nitrogen adsorption–desorption isotherms (with the BJH pore size distributions plots in the insets) measured at 77 K for the (a) NiO–$NaBH_4$ and (b) NiO–NaOH.

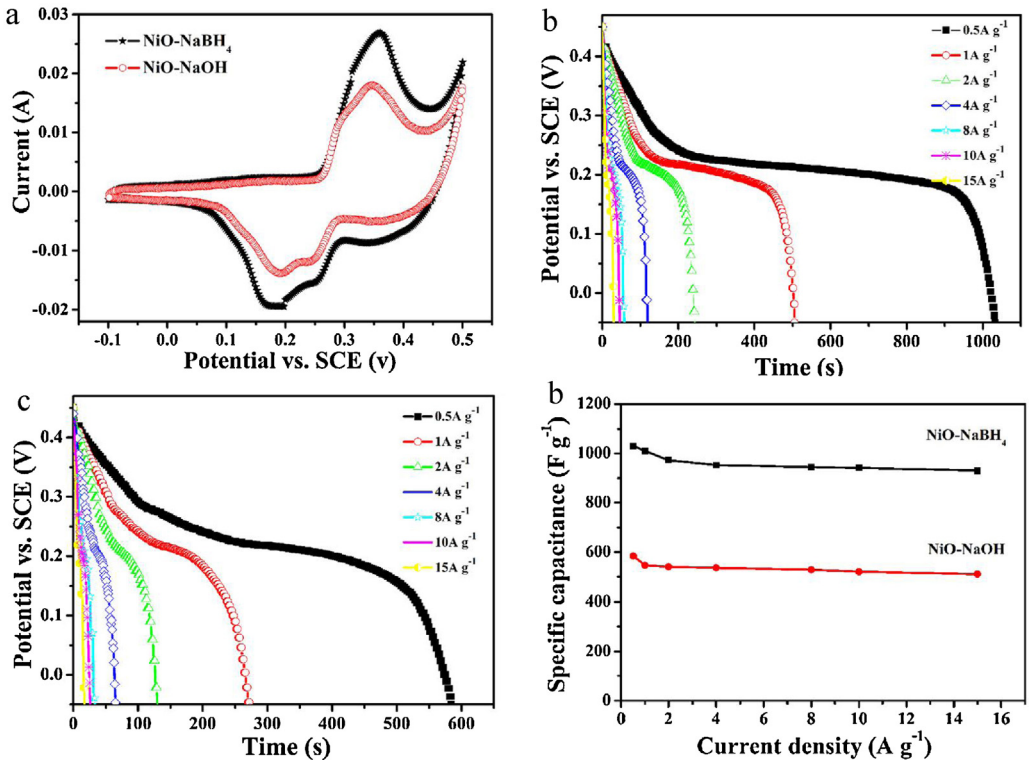

Fig. 7. Electrochemical characterizations of NiO: (a) CV curves at a scan rate of 5 mV s^{-1}. Galvanostatic charge–discharge curves of NiO–$NaBH_4$ (b) and NiO–NaOH (c) at different current density. (d) Average specific capacitance at different current density.

Table 1
Summary of electrochemical data of NiO based electrodes. Complete data can be found in the literature.

Samples	Technique	Surface area ($m^2 g^{-1}$)	Capacitance ($F g^{-1}$)	Electrolyte	Current load or scan rate	Ref.
NiO	Microwave	125	598	1 M KOH	5 mV s^{-1}	[14]
NiO	Microwave	176	585	2 M KOH	5 A g^{-1}	[16]
NiO array	Hydrothermal		2018	1 M NaOH	2.27 A g^{-1}	[17]
NiO	Hydrothermal	85.18	348	2 M KOH	5 mV s^{-1}	[19]
NiO	Hydrothermal	102.4	390	1 M KOH	5 A g^{-1}	[29]
NiO	Reflux	216	710	6 M KOH	1 A g^{-1}	[30]
NiO	Hydrothermal	215.3	555	6 M KOH	1 A g^{-1}	[31]
NiO	Reflux	258.52	718	6 M KOH	2 mV s^{-1}	[32]
NiO	Hydrothermal	265	279	2 M KOH	5 mV s^{-1}	[41]
NiO	Reflux	414	930	2 M KOH	15 A g^{-1}	This work

3.4. Electrochemical characterization

The CV measurements of NiO–$NaBH_4$ and NiO–NaOH (Fig. 7a) were recorded at 5 mV s^{-1} in the potential range of −0.1 to 0.5 V. The anodic and cathodic peaks corresponded to the reversible reaction of Ni^{2+}/Ni^{3+}, which provides active center for generating pseudocapacitance [39]. From the CV curves, we can easily figure out that the capacitance of NiO–$NaBH_4$ is much higher than that of NiO–NaOH.

To further study the electrochemical performance of both the samples, galvanostatic charge/discharge measurements were carried out. Fig. 7b and c shows the galvanostatic discharge curves of NiO–$NaBH_4$ and NiO–NaOH at various current densities in a potential window of −0.05 to 0.45 V. All the curves are nonlinear, suggesting pseudocapacitance behavior of NiO samples. Based on galvanostatic discharge curves, the specific capacitances were calculated. As determined in Fig. 7d, the specific capacitance values of NiO–$NaBH_4$ are respectively 1030, 1010, 972, 952, 944, 940, and 930 F g^{-1} at 0.5, 1, 2, 4, 8, 10 and 15 A g^{-1}. For NiO–NaOH, the values are 584, 540, 520, 528, 528, 520, and 510 F g^{-1}. It is noteworthy that NiO–$NaBH_4$ presents higher capacitance compared with NiO–NaOH at all current densities. The specific capacitance of NiO–$NaBH_4$ is comparable to those of the previously reported data in literature for NiO based materials (Table 1). This is ascribed to its large specific surface areas and appropriate pore size. To further investigate the conductivity of electrode materials, both NiO samples were subjected to AC impedance measurements between 0.01 and 1×10^5 Hz.

Fig. 8 exhibits the complex-plane impedance plots of the NiO electrodes with potential amplitude of 0.2 V. As shown in the enlarged view, there are two arcs in the high and medium frequency regions. The arc of high frequency can be attributed to the resistance arising from the discontinuity of conductivity at the electrode–electrolyte interface [40,41]. The arc diameter of

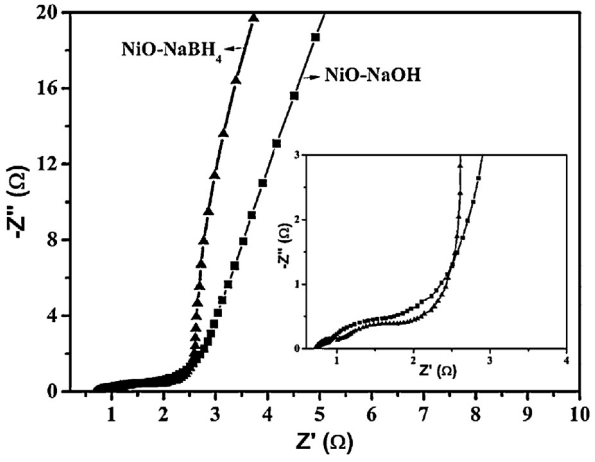

Fig. 8. Complex plane impedance plots of NiO–$NaBH_4$ and NiO–NaOH.

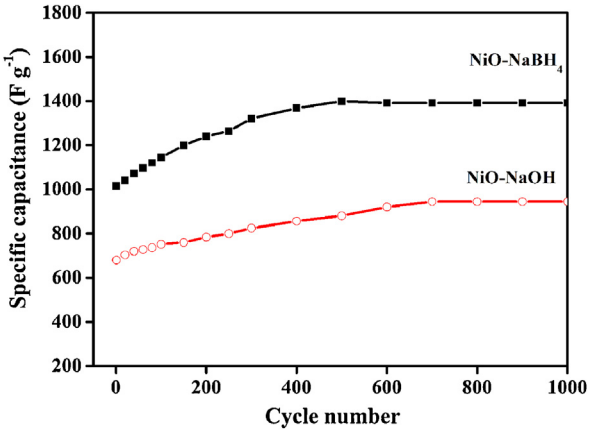

Fig. 9. Cyclic performance of NiO at 4 A g^{-1}.

NiO–NaOH is smaller than that of NiO–$NaBH_4$, revealing its higher conductivity. The impedance behavior of the NiO electrodes in the medium frequency regions can be explained as the Faradic charge-transfer resistance during the surface redox reaction. The charge-transfer resistance value associates with the surface properties of active materials. It can be seen that the value of NiO–$NaBH_4$ electrode is lower than that of NiO–NaOH electrode. This is ascribed to the larger specific surface area and spherical spongy morphology of NiO–$NaBH_4$. Because the special porous structure provides more sites to bond conductive acetylene black, which is beneficial to charge transfer. The linear tails in the plot at the low frequency derive from the transportation of OH ions within the channels of NiO electrode during redox reactions. Compared with NiO–NaOH, NiO–$NaBH_4$ electrode shows distinctive near-straight vertical line, demonstrating lower diffusion resistance. It is reasonable because flakelet-like porous structure of NiO–$NaBH_4$ is helpful to the diffusion of the OH ions. In general, NiO synthesized by $NaBH_4$ possesses more effective specific areas and is more suitable to supercapacitor applications.

As we know, the circle lifespan is a key factor to evaluate electrode materials. Hence, the cycle performance of NiO samples was collected at 4 A g^{-1} (Fig. 9). In the first several hundred cycles, the specific capacitance of both NiO increases. This can be attributed to the penetration of electrolyte ions and gradual activation of the active materials. After 1000-cycle test, the specific capacitance of NiO–$NaBH_4$ achieves 1396 F g^{-1}. These results reveal that the high specific capacitance and excellent cycle stability are achieved in NiO–$NaBH_4$ for supercapacitors.

4. Conclusion

In summary, NiO, a low-cost porous material of high specific surface areas, has been prepared by a simple reflux process using $NaBH_4$ dissolved in ethylene glycol as a novel precipitant. The

porous NiO exhibits a high specific capacitance of 1396 F g^{-1} after 1000 cycles and shows excellent rate performance and long cycle life. From this work, we open up a viewpoint that $NaBH_4$-EG can be used as weak alkaline precipitant. This finding can be extended to the preparation of other materials.

Acknowledgements

This work is supported by the National Basic Research Program of China (2012CB932303) and the National Natural Science Foundation of China (Grant No. 51172261).

Appendix A. Supplementary data

Supplementary data associated with this article can be found, in the online version, at http://dx.doi.org/10.1016/j.electacta.2013.05.122.

References

[1] H.L. Wang, Q.M. Gao, J. Hu, High Hydrogen Storage Capacity of Porous Carbons Prepared by Using Activated Carbon, Journal of the American Ceramic Society 131 (2009) 7016–7022.
[2] S.B. Yang, X.L. Feng, S. Ivanovici, K. Müllen, Fabrication of Graphene-Encapsulated Oxide Nanoparticles: Towards High-Performance Anode Materials for Lithium Storage, Angewandte Chemie International Edition 49 (2010) 8408–8411.
[3] X. Wang, L.J. Zhi, K. Müllen, Transparent, Conductive Graphene Electrodes for Dye-Sensitized Solar Cells, Nano Letters 8 (2008) 323–327.
[4] Z.Y. Wang, L. Zhou, X.W. Lou, Metal Oxide Hollow Nanostructures for Lithium-ion Batteries, Advanced Materials 24 (2012) 1903–1911.
[5] H. Chang, S.H. Joo, C. Pak, Synthesis and characterization of mesoporous carbon for fuel cell applications, Journal of Materials Chemistry 17 (2007) 3078–3088.
[6] X.Y. Lang, A. Hirata, T. Fujita, M.W. Chen, Nanoporous metal/oxide hybrid electrodes for electrochemical supercapacitors, Nature Nanotechnology 6 (2011) 232–236.
[7] H. Jiang, P.S. Lee, C.Z. Li, 3D carbon based nanostructures for advanced supercapacitors, Energy & Environmental Science 6 (2013) 41–53.
[8] J.T. Zhang, J.W. Jiang, H.L. Li, X.S. Zhao, Ultralong single crystalline V_2O_5 nanowire/graphene composite fabricated by a facile green approach and its lithium storage behavior, Energy & Environmental Science 4 (2011) 4009–4015.
[9] J.P. Liu, J. Jiang, C.W. Cheng, H.X. Li, H. Gao, H.J. Fan, Co_3O_4 Nanowire@MnO_2 Ultrathin Nanosheet Core/Shell Arrays: A New Class of High-Performance Pseudocapacitive Materials, Advanced Materials 23 (2011) 2076–2081.
[10] X. Sun, G.K. Wang, J.Y. Hwang, J. Lian, Porous nickel oxide nano-sheets for high performance pseudocapacitance materials, Journal of Materials Chemistry 21 (2011) 16581–16588.
[11] G.P. Wang, L. Zhang, J.J. Zhang, A review of electrode materials for electrochemical supercapacitors, Chemical Society Reviews 41 (2012) 797–828.
[12] J.J. Xu, K. Wang, S.Z. Zu, B.H. Han, Z.X. Wei, Hierarchical Nanocomposites of Polyaniline Nanowire Arrays on Graphene Oxide Sheets with Synergistic Effect for Energy Storage, ACS Nano 4 (2010) 5019–5026.
[13] C.C. Hu, W.C. Chen, K.H. Chang, How to achieve maximum utilization of hydrous ruthenium oxide for supercapacitors, Journal of the Electrochemical Society 151 (2004) 281–290.
[14] S.K. Mether, P. Justin, G.R. Rao, Microwave-Mediated Synthesis for Improved Morphology and Pseudocapacitance Performance of Nickel Oxide, ACS Applied Materials & Interfaces 3 (2011) 2063–2073.
[15] M.W. Xu, S.J. Bao, H.L. Li, Synthesis and characterization of mesoporous nickel oxide for electrochemical capacitor, Journal of Solid State Electrochemistry 11 (2007) 372–377.
[16] C.Y. Cao, W. Guo, Z.M. Cui, W.G. Song, W. Cai, Microwave-assisted gas/liquid interfacial synthesis of flowerlike NiO hollow nanosphere precursors and their application as supercapacitor electrodes, Journal of Materials Chemistry 21 (2011) 3204–3209.
[17] Z.Y. Lu, Z. Chang, J.F. Liu, X.M. Sun, Stable ultrahigh specific capacitance of NiO nanorod arrays, Nano Research 4 (2011) 658–665.
[18] X.H. Xia, J.P. Tu, Y.J. Mai, R. Chen, X.L. Wang, C.D. Gu, X.B. Zhao, Graphene Sheet/Porous NiO Hybrid Film for Supercapacitor Applications, Chemistry-A European Journal 17 (2011) 10898–10905.
[19] D.W. Su, H.S. Kim, W.S. Kim, G.X. Wang, Mesoporous Nickel Oxide Nanowires: Hydrothermal Synthesis, Characterisation and Applications for Lithium-Ion Batteries and Supercapacitors with Superior Performance, Chemistry-A European Journal 18 (2012) 8224–8229.
[20] H.L. Wang, H.S. Casalongue, Y.Y. Liang, H.J. Dai, $Ni(OH)_2$ Nanoplates Grown on Graphene as Advanced Electrochemical Pseudocapacitor Materials, Journal of the American Ceramic Society 132 (2010) 7472–7477.
[21] S.B. Yang, X.L. Wu, C.L. Chen, H.L. Dong, W.P. Hu, X.K. Wang, Spherical α-$Ni(OH)_2$ nanoarchitecture grown on graphene as advanced electrochemical pseudocapacitor materials, Chemical Communications 48 (2012) 2773–2775.
[22] Z. Tang, C.H. Tang, H. Gong, A High Energy Density Asymmetric Supercapacitor from Nano-architectured $Ni(OH)_2$/Carbon Nanotube Electrodes, Advanced Functional Materials 22 (2012) 1272–1278.
[23] H. Jiang, T. Zhao, C.Z. Li, J. Ma, Hierarchical self-assembly of ultrathin nickel hydroxide nanoflakes for high-performance supercapacitors, Journal of Materials Chemistry 21 (2011) 3818–3823.
[24] H.T. Wang, L. Zhang, X.H. Tan, C.M.B. Holt, B. Zahiri, B.C. Olsen, D. Mitlin, Supercapacitive Properties of Hydrothermally Synthesized Co_3O_4 Nanostructures, Journal of Physical Chemistry C 115 (2011) 17599–17605.
[25] R.B. Rakhi, W. Chen, D. Cha, H.N. Alshareef, Substrate dependent self-organization of mesoporous cobalt oxide nanowires with remarkable pseudocapacitance, Nano Letters 12 (2012) 2559–2567.
[26] H. Lee, J. Kang, M.S. Cho, J.B. Choic, Y. Lee, MnO_2/graphene composite electrodes for supercapacitors: the effect of graphene intercalation on capacitance, Journal of Materials Chemistry 21 (2011) 18215–18219.
[27] D.L. Yan, Z.L. Guo, G.S. Zhu, Z.Z. Yu, H. Xu, A.B. Yu, MnO_2 film with three-dimensional structure prepared by hydrothermal process for supercapacitor, Journal of Power Sources 199 (2012) 409–412.
[28] T.Y. Wei, C.H. Chen, H.C. Chien, S.Y. Lu, C.C. Hu, A Cost-Effective Supercapacitor Material of Ultrahigh Specific Capacitances: Spinel Nickel Cobaltite Aerogels from an Epoxide-Driven Sol-Gel Process, Advanced Materials 22 (2010) 347–351.
[29] X.J.W.H. Zhang, Shi J.X. Zhu, W.Y. Zhao, J. Ma, S. Mhaisalkar, T.L. Maria, Y.H. Yang, H. Zhang, H.H. Hng, Q.Y. Yan, Synthesis of porous NiO nanocrystals with controllable surface area and their application as supercapacitor electrodes, Nano Research 3 (2010) 643–652.
[30] C.Z. Yuan, X.G. Zhang, L.H. Su, B. Gao, L.F. Shen, Facile synthesis and self-assembly of hierarchical porous NiO nano/micro spherical superstructures for high performance supercapacitors, Journal of Materials Chemistry 19 (2009) 5772–5777.
[31] X.W. Li, S.L. Xiong, J.F. Li, J. Bai, Y.T. Qian, Mesoporous NiO ultrathin nanowire networks topotactically transformed from α-$Ni(OH)_2$ hierarchical microspheres and their superior electrochemical capacitance properties and excellent capability for water treatment, Journal of Materials Chemistry 22 (2012) 14276–14283.
[32] J.W. Lee, T. Ahn, J.H. Kim, J.M. Ko, J.D. Kim, Nanosheets based mesoporous NiO microspherical structures via facile and template-free method for high performance supercapacitors, Electrochimica Acta 56 (2011) 4849–4857.
[33] X.M. Ni, Y.F. Zhang, D.Y. Tian, H.G. Zheng, X.W. Wang, Synthesis and characterization of hierarchical NiO nanoflowers with porous structure, Journal of Crystal Growth 306 (2007) 418–421.
[34] L.P. Zhu, G.H. Liao, Y. Yang, H.M.J. Xiao, F. Wang, S.Y. Fu, Self-assembled 3D flower-like hierarchical -$Ni(OH)_2$ hollow architectures and their in situ thermal conversion to NiO, Nanoscale Research Letters 4 (2009) 550–557.
[35] Q. Lu, M.W. Lattanzi, Y.P. Chen, X.M. Kou, W.F. Li, X. Fan, K.M. Unruh, J.G. Chen, J.Q. Xiao, Supercapacitor Electrodes with High-Energy and Power Densities Prepared from Monolithic NiO/Ni Nanocomposites, Angewandte Chemie International Edition 50 (2011) 6847–6850.
[36] Y. Wang, X. Jiang, Y. Xia, Formation of $ZnMn_2O_4$ Ball-in-Ball Hollow Microspheres as a High-Performance Anode for Lithium-Ion Batteries, Journal of the American Ceramic Society 125 (2003) 16176–16177.
[37] A.M. Cao, J.S. Hu, H.P. Liang, L.J. Wan, Self-Assembled Vanadium Pentoxide (V_2O_5) Hollow Microspheres from Nanorods and Their Application in Lithium-Ion Batteries, Angewandte Chemie International Edition 44 (2005) 4391–4395.
[38] P. Simon, Y. Gogotsi, Materials for electrochemical capacitors, Nature Materials 7 (2008) 845–854.
[39] J.W. Lang, L.B. Kong, W.J. Wu, Y.C. Luo, L. Kang, Facile approach to prepare loose-packed NiO nano-flakes materials for supercapacitors, Chemical Communications 35 (2008) 4213–4215.
[40] S.K. Meher, G.R. Rao, Effect of Microwave on the Nanowire Morphology, Optical, Magnetic, and Pseudocapacitance Behavior of Co_3O_4, Journal of Physical Chemistry C 115 (2011) 25543–25556.
[41] S.K. Meher, P. Justin, G.R. Rao, Nanoscale morphology dependent pseudocapacitance of NiO: Influence of intercalating anions during synthesis, Nanoscale 3 (2011) 683–692.